Agricultural Water Management 324 (2026) 110137

Contents lists available at ScienceDirect

Agricultural Water Management

journal homepage: www.elsevier.com/locate/agwat

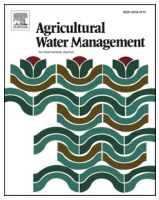

Shifting climatic sensitivities of drought-related yield gaps signal potential increases in irrigation reliance in the Yellow River Basin

Linchao Li [a,b,c], Zhongshan Xu [a,*], Yajie Zhang [d], Ning Yao [b,e], Yi Li [e], Qiang Yu [b], Hao Feng [b], Guijun Yang [f,g], Qinsi He [c,h,**]

[a] College of Agronomy, Inner Mongolia Agricultural University, Hohhot 010019, China
[b] State Key Laboratory of Soil and Water Conservation and Desertification Control, Northwest A&F University, Yangling, Shaanxi 712100, China
[c] State Key Laboratory of Water Engineering Ecology and Environment in Arid Area, Inner Mongolia Agricultural University, Hohhot 010018, China
[d] State Key Laboratory of Environmental Criteria and Risk Assessment, Chinese Research Academy of Environmental Science, No. 8 Anwai Dayangfang, Beijing 100012, China
[e] College of Water Resources and Architectural Engineering, Northwest A&F University, Yangling, Shaanxi 712100, China
[f] College of Geological Engineering and Geomatics, Chang'an University, Xi'an 710054, China
[g] Key Laboratory of Quantitative Remote Sensing in Agriculture of Ministry of Agriculture and Rural Affairs, Information Technology Research Center, Beijing Academy of Agriculture and Forestry Sciences, Beijing 100097, China
[h] College of Water Conservancy and Civil Engineering, Inner Mongolia Agricultural University, Hohhot 010018, China

ARTICLE INFO

Keywords:
Crop model
Drought risk
Global warming
Machine learning
Sensitivity analysis

ABSTRACT

Climate change is intensifying drought risk and threatening food production, yet how drought-driven yield losses evolve with warming remains poorly quantified. Here, we combine an ensemble of nine crop models with 38 global climate models to quantify shifting sensitivities of the irrigated–rainfed yield gap to key climate drivers across the Yellow River Basin under SSP126, SSP245, and SSP585. We find that yield gaps increase for maize, soybean, and rice under future climates, while wheat exhibits a slight decrease. The precipitation is negatively associated with the yield gap, but this negative effect weakens (shifts toward zero) across large areas of the basin. For maize, 69.8 %, 66.7 %, and 77.8 % of grid cells show increasing sensitivity under SSP126, SSP245, and SSP585, respectively. This indicates rainfall is becoming less effective at narrowing the gap as atmospheric demand rises, implying greater reliance on irrigation. Evapotranspiration (ET) generally shows the opposite spatial pattern, except in some extremely arid upstream areas where ET-yield gap coupling weakens or even decouples due to high atmospheric demand. Yield gap sensitivity to atmospheric CO_2 is negative in most regions, consistent with improved water-use efficiency that reduces the yield gap; this effect is more pronounced in the arid upstream. By identifying spatiotemporal hotspots of intensifying yield-gap sensitivities, this study informs targeted irrigation investment and drought-time water-allocation prioritization, supporting climate-smart water management to stabilize production and long-term sustainability.

1. Introduction

Drought is one of the most critical climatic stresses threatening global food security (Krishnamurthy R et al., 2022). The increasing frequency and intensity of extreme drought events under climate change profoundly alter the hydrological cycle and reduce agricultural water availability (Allan et al., 2020; Greve and Seneviratne, 2015), thereby posing serious risks to crop production and food security (Wang et al., 2024b). Irrigation plays a vital role in buffering drought impacts and sustaining crop yields (Wang et al., 2021). However, the expansion of irrigation and irrigated cropland can impact regional water cycles, water availability, and exacerbate pressure on limited freshwater resources (Mehta et al., 2024). Therefore, a better understanding of how climatic drought affects crop yields and the underlying driving factors is crucial for achieving sustainable irrigation management and improving water productivity (Bo et al., 2024; Zhang et al., 2021).

* Corresponding author.
** Corresponding author at: State Key Laboratory of Water Engineering Ecology and Environment in Arid Area, Inner Mongolia Agricultural University, Hohhot 010018, China.
E-mail addresses: xzs1992@imau.edu.cn (Z. Xu), qinsihe@outlook.com (Q. He).

https://doi.org/10.1016/j.agwat.2026.110137
Received 16 November 2025; Received in revised form 5 January 2026; Accepted 6 January 2026
Available online 15 January 2026

Drought risk is projected to increase under climate change (Yao et al., 2020), further amplifying the likelihood of yield losses and dependence on irrigation. For instance, rising potential evapotranspiration (PET) accounts for approximately 60 % of the area experiencing heightened drought risk, driven by intensified interactions between soil moisture and atmospheric water demand in the Yellow River Basin (Wang et al., 2022b). However, on the other hand, increasing CO_2 increases photosynthesis in crops (especially for C_3 crops) by promoting Rubisco activity and reducing photorespiration, while also lowering stomatal conductance (Toreti et al., 2020). This process improves water-use efficiency (WUE) and can potentially compensate for drought stress (Swann et al., 2016). In addition, CO_2 fertilization is crop-specific and is generally stronger for C3 crops (e.g., wheat, soybean, rice) than for C4 crops (e.g., maize), indicating CO_2 and precipitation-driven changes in yield-gap sensitivity differ among crops. Thus, such countervailing forces indicate that the coupling between climate and yield is evolving in space and time. Although some studies have explored the impacts of drought on crop productivity (Kamali et al., 2022; Santini et al., 2022), few studies have investigated how the sensitivity of crop yields to drought evolves with climate change. Clarifying these dynamics is essential for reducing uncertainty in drought impact assessments and for developing strategies that guide the long-term sustainable management of agricultural irrigation.

To quantify drought impacts on crop yields in arid regions, some previous studies relied on statistical models using field survey or regional yield data (Li et al., 2022; Santini et al., 2022). However, these approaches may not fully capture drought risk because yield losses in irrigated areas are largely buffered. Process-based crop models have also been used to analyze the relationships between crop yields and drought indices (Chen et al., 2020; Leng and Hall, 2019), but such studies may underestimate drought impacts in irrigated regions where water supply partially mitigates stress. In contrast, the yield gap between irrigated and rainfed conditions provides a more direct measure of drought impact, reflecting how water limitation constrains potential yields under different drought intensities (Hou et al., 2024; Wang et al., 2021). This approach has been used to evaluate drought effects across various regions (Li and Troy, 2018). However, how the yield gap changes under climate change, what dominant factors influence it, and how these drivers evolve through time remain poorly understood, particularly in irrigated agricultural systems.

The Yellow River Basin (YRB) is China's second-largest river basin, that largely located in arid and semi-arid zones. It is a national breadbasket that contributes around 13 % of China's crop production while having only around 2 % of the country's water resources (YRCC, 2019; Zhuo et al., 2022). Drought is one of the dominant natural hazards in the YRB, and much of its agriculture depends on irrigation (Wang et al., 2025). Therefore, quantifying drought risk and identifying how specific climatic drivers that determine it are essential for developing sustainable agricultural management and strengthening the Yellow River Basin's food-system resilience to drought.

Here, we combine an ensemble of nine process-based crop models with 38 global climate models to simulate irrigated and rainfed yields of maize, wheat, soybean, and rice across the Yellow River Basin under historical and Shared Socioeconomic Pathways (SSP) scenarios. We quantify drought impacts using the irrigated–rainfed yield gap, where irrigated yields represent no water stress and rainfed yields depend on precipitation; thus, the gap mainly reflects yield losses attributable to water limitation (drought stress). Key climatic drivers are identified by machine-learning attribution, and time-varying sensitivities are assessed with a dynamic linear model (Fig. 1). Our objectives are to: (1) project future crop yields under climate change; (2) estimate how the irrigated-rainfed yield gap changes over time; (3) identify the main climatic

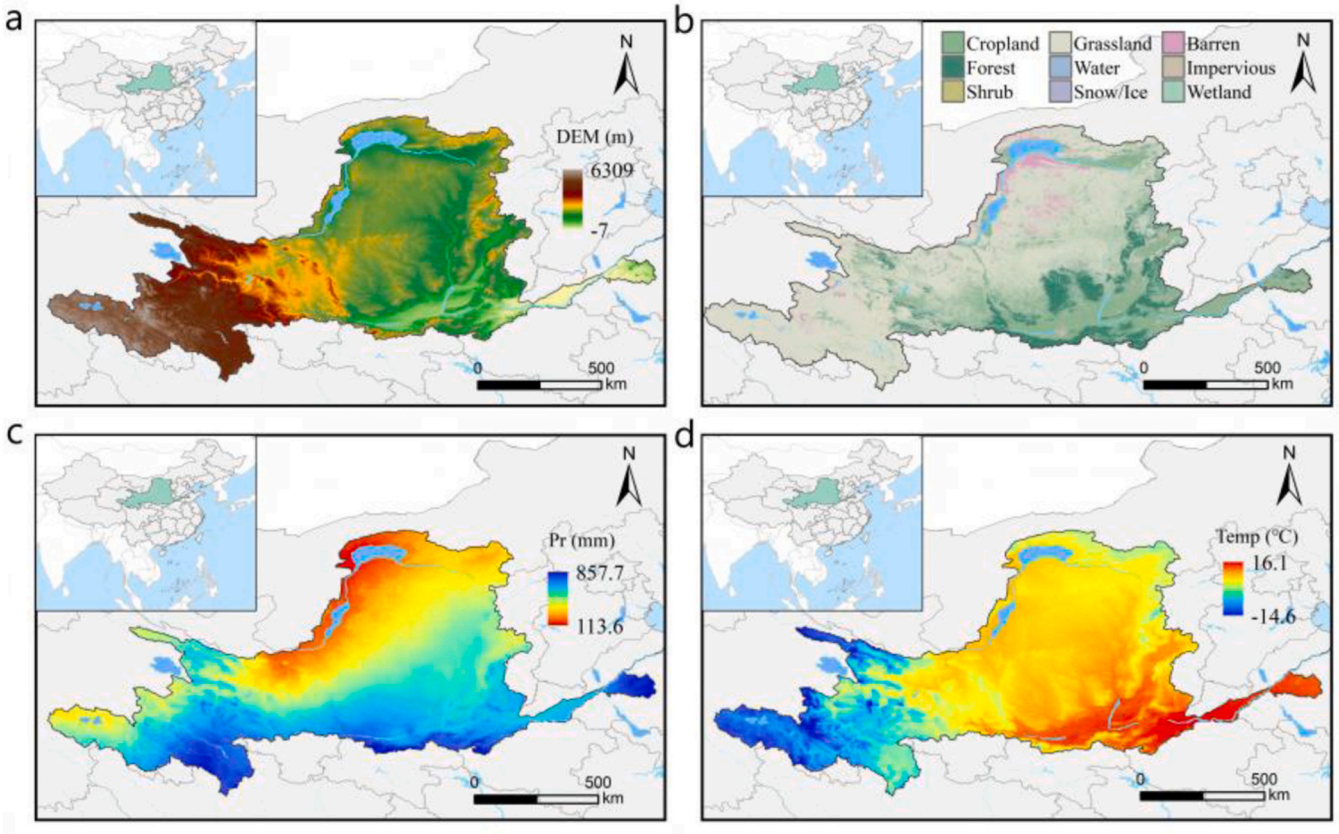

Fig. 1. Spatial characteristics of the study area (Yellow River Basin). a, Digital elevation model (DEM); b, land-use and land-cover distribution; c, spatial pattern of annual precipitation; d, spatial patterns of air temperature. Pr, precipitation; Temp, Temperature.

factors influencing the yield gap; and (4) reveal trends in crop yield sensitivity to these factors across scenarios. Our study offers a process-based perspective on how climatic drought affects crop yields, with clear implications for developing sustainable irrigation management and narrowing uncertainties about drought impacts on food production in irrigated agricultural regions.

2. Data and methods

2.1. Study area and data

The Yellow River Basin (YRB; 95°53′E-119°5′E; 32°10′N-41°50′N) in northern China spans arid, semi-arid, and semi-humid zones. It extends around 5464 km from headwaters on the Tibetan Plateau to the North China Plain and covers around 752,443 km^2 (Niu et al., 2024). Precipitation increases markedly from northwest to southeast, with mean annual total precipitation from 100 to 860 mm (Fig. 1). Mean annual air temperature ranges from about −15 °C to 16 °C, generally decreasing from east to west with rising elevation. The basin is drought-prone, and stable crop production relies heavily on irrigation.

The observed climate data in this study were collected from Peng et al. (2019), developed by delta spatial downscaling of CRU time series with WorldClim climatology (bilinear interpolation). Observed gridded crop yields for maize, wheat, soybean, and rice were obtained from Cao et al. (2025), derived from multi-source inputs using machine-learning methods. Monthly precipitation and temperature under future climate scenarios were collected from CMIP6 with the 38 Global Climate Models (GCMs) under SSP126, SSP245, and SSP585 (Table S1). We used this large multi-model ensemble to span a wide range of crop-model structures and CMIP6 climate projections, thereby capturing diverse representations of crop responses and climate uncertainty across the YRB. The selected CMIP6 GCMs were selected to span a wide range of equilibrium climate sensitivity (ECS) and associated hydroclimatic responses, including low-ECS models (e.g., NorESM2-MM), mid-range models (e.g., MPI-ESM1–2-LR), and high-ECS models (e.g., UKESM1–0-LL and HadGEM3-GC31-LL). All datasets were harmonized to a 5-arc-minute grid using bilinear resampling based on the high-resolution harvest--area datasets (Monfreda et al., 2008; Portmann et al., 2010). Land-use change and socio-economic dynamics that may affect future irrigation capacity (e.g., infrastructure investment, technology adoption, and water-supply constraints) were not represented.

2.2. Global gridded crop model emulators

Future crop yields under climate change were projected using emulators of global gridded crop models (GGCMs) (Franke et al., 2020b). These emulators represent crop responses to carbon dioxide concentration (C), air temperature (T), water conditions (W; irrigation and precipitation), and nitrogen input (N) within a static framework that effectively reproduces yield changes across environmental conditions (Franke et al., 2020a, 2020b). Because our analysis focuses on drought-related yield impacts, nitrogen inputs were set to 200 kg N ha^{-1} , with crop growth assumed to be free of nitrogen limitation. Our ensemble integrates nine crop models for wheat and maize (CARAIB, EPIC-TAMU, JULES, GEPIC, LPJ-GUESS, LPJmL, pDSSAT, PEPIC, PROMET) and eight for rice and soybean (CARAIB, EPIC-TAMU, JULES, GEPIC, LPJmL, pDSSAT, PEPIC, PROMET). The crop models are driven by outputs from 38 CMIP6 global climate models, spanning a wide range of climate sensitivities and precipitation–temperature trajectories (Meehl et al., 2020). Because the emulators are driven by relative changes in GCM variables, no bias correction of the GCM fields is required (Li et al., 2023a; Müller et al., 2021). The drought impact metric was estimated as the irrigated-rainfed yield difference (yield gap), which was used in all subsequent sensitivity analyses. To better reflect the spatial heterogeneity and temporal evolution of drought impacts across grids with different baseline productivity, we additionally present a rainfed-normalized yield-gap index for mapping and comparison:

$$Y_{gap} = \frac{Y_{irrigated} - Y_{rainfed}}{Y_{rainfed}} \times 100\% \quad (1)$$

Where Y_{gap} is the crop yield gaps, $Y_{irrigated}$ is the irrigated yield, and $Y_{rainfed}$ is the rainfed yield. We normalized the yield gaps by rainfed-yield to facilitate spatial comparison across grids with different baseline productivity and to retain an intuitive interpretation in which larger values indicate stronger relative water limitation (i.e., larger proportional irrigation benefits). In this study, we use the yield-gap/Y_{rainfed} (rather than yield-gap/$Y_{irrigated}$) because rainfed yield provides a locally relevant water-limited baseline, making the ratio easier to interpret as drought-related yield loss relative to local rainfed conditions. Note that this normalized index is used to present the spatiotemporal patterns of yield-gap evolution, whereas the attribution and sensitivity analyses are based on the absolute yield difference. Moreover, in this framework, the yield gap is interpreted as a biophysical indicator of water-limitation alleviation under irrigation; socio-economic constraints on irrigation capacity (e.g., irrigation policy or infrastructure limitations) are not represented and may confound real-world reliance.

2.3. Statistical downscaling

Since the 38 GCMs have coarse resolution, we applied statistical downscaling to better resolve relationships between the yield gap and climatic drivers. Monthly GCM outputs were first bilinearly resampled to a 5-arc-minute grid and then bias-corrected using the delta method. We first bilinearly resampled each GCM field to 5-arc-minute. Bias correction used the delta method relative to 1980–2010, treating variables additively within the growth season. For each variable X(temperature or precipitation), the monthly bias was computed as

$$D = X_{GCMs} - X_{obs} \quad (2)$$

and the bias-corrected (downscaled) field was obtained as

$$XSD = XGCMs - D \quad (3)$$

Where X_{GCM} is the temperature or precipitation from the GCM outputs; X_{obs} denotes temperature or precipitation from the observed dataset (Peng et al., 2019); X_{SD} is the statistically downscaled data.

Because GGCM emulator baseline yields differ from observation-based yields, we applied a yield bias correction to align absolute baseline yield levels with observed data. Emulator outputs were first bilinearly resampled from 0.5° × 0.5° to a 5-arc-minute grid. For each crop model, we then computed fractional yield changes between the baseline (1982–2010) and each future period (2021–2099) and applied these factors to the observational reference yields to generate bias-corrected projections (Jägermeyr et al., 2021). Details of the observed yield dataset are provided in Cao et al. (2025).

2.4. Statistical models

2.4.1. The random forest

We used a random forest (RF) model to identify the dominant drivers of the yield gap, considering atmospheric CO_2, standardized precipitation–evapotranspiration index (SPEI), precipitation, and ET (calculated using the Thornthwaite 1948 method). RF can capture both linear and nonlinear relationships between predictors and responses (Breiman, 2001; Feng et al., 2019). In this study, a random forest model was fitted for each grid cell in R (version 4.1.1; R Core Team; R Foundation for Statistical Computing, Vienna, Austria), and variable-importance values were normalized to sum to 100 %. We assessed the dominant impact factors for the baseline (1980–2010) and the future period (2069–2099) across SSP126, SSP245, and SSP585. Random forest models were fitted separately for each grid cell to quantify the relative importance of

climatic drivers. Because hyperparameter tuning for each cell is computationally infeasible at this scale, we adopted stable default settings (m_{try}=3, n_{tree}=500), which are sufficient for robust importance ranking in regression applications.

2.4.2. Dynamic linear model

The random forest model identifies the magnitude of each driver's contribution to the yield gap but does not provide the direction of effect at each grid cell (positive versus negative). To quantify directional, time-varying effects, we employ a dynamic linear model (DLM), which estimates the sensitivity of crop yield gaps to individual climatic variables. Compared with a standard multiple linear regression, the DLM accommodates time-varying coefficients and temporal dependence in the residuals, making it well suited to time-series regression (Prado and West, 2010). This allows us to reveal trends in the sensitivity of irrigated–rainfed yield gaps to precipitation, temperature, SPEI, and CO_2 under changing climate conditions. The DLM has been applied widely in Earth system science, environmental change, and agriculture (Li et al., 2023b; Liu et al., 2019; Zhang et al., 2022). We fit a separate DLM for each grid cell for the baseline (1980–2010) and the future period (2069–2099) across SSP126, SSP245, and SSP585, consistent with the RF. To quantify long-term changes, we also test for linear trends in sensitivities expressed per decade (10a) during 1980–2099 under SSP126, SSP245, and SSP585. Since all climatic factors are included jointly in the DLM, the estimated sensitivities quantify conditional marginal effects on the yield gap, rather than isolated single-factor responses. Consequently, co-variability among predictors may influence individual coefficients through shared variance and should be considered when interpreting single-variable sensitivities. Although the RF attribution and the DLM are well-suited for this study, dominant-driver identification and sensitivity estimates may still involve methodological uncertainty. An inter-method comparison and uncertainty analysis across different statistical models (e.g., multiple linear regression and other machine-learning approaches) is beyond the scope of this work but represents valuable directions for future study.

Generally, using the methods described above, we quantified changes in the yield gap under future scenarios and revealed trends in its sensitivity to climatic drivers. This modeling and analytical framework is transferable to other irrigated regions, provided that comparable irrigated and rainfed yield estimates and climate-driver data are available. An overview of the analytical methodology is shown in Fig. 2.

3. Results

3.1. Projected crop yield change

We projected spatial patterns of crop yields for 2069–2099 relative to the baseline (1980–2010) under SSP126, SSP245, and SSP585 in the

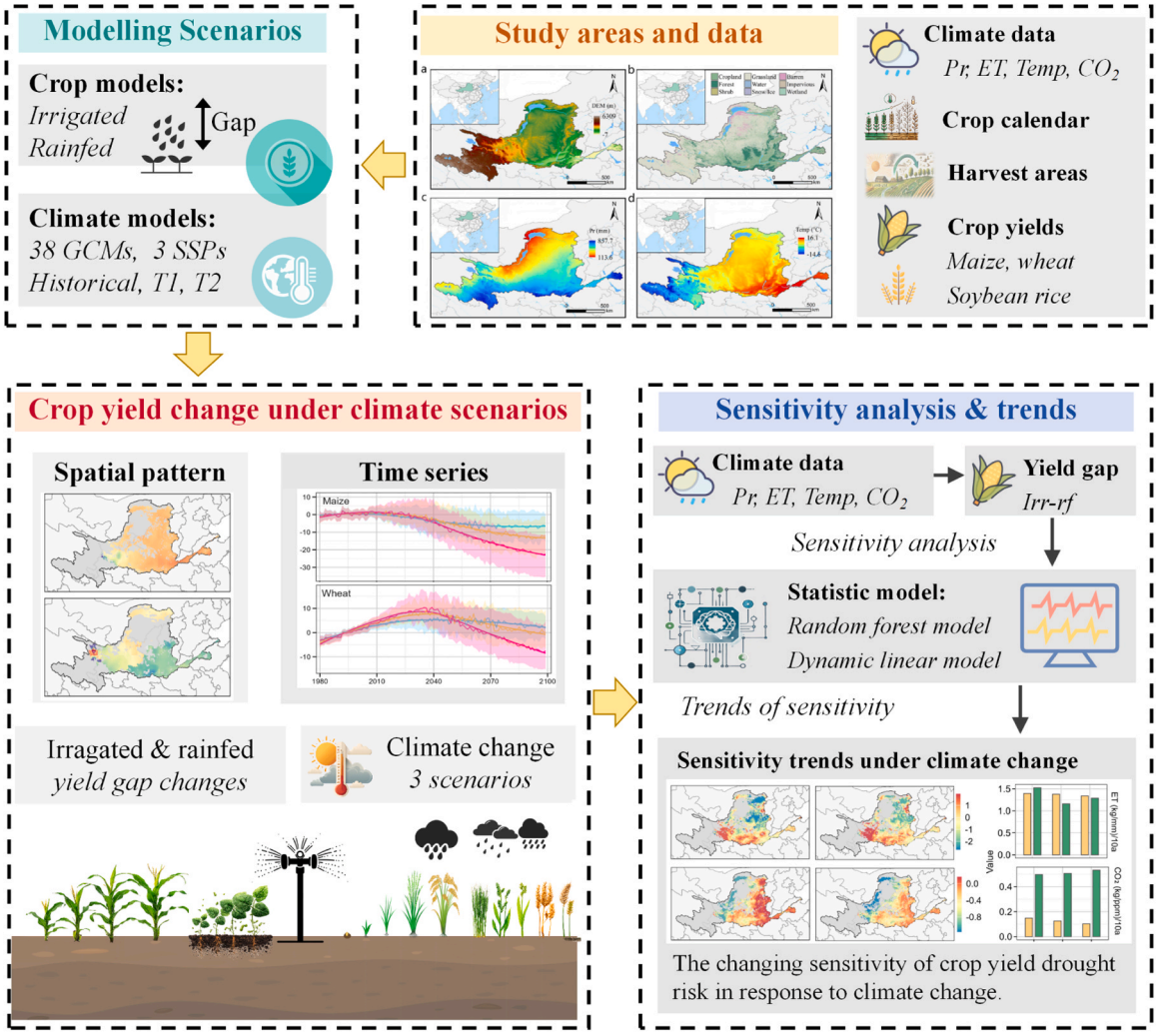

Fig. 2. Overview of the analytical framework for quantifying drought impacts on crop yields and their climatic attribution under climate change. Pr, precipitation; Temp, temperature; ET, evapotranspiration; CO_2, atmospheric carbon dioxide; Irr, irrigated; rf, Rainfed; SSP, Shared Socioeconomic Pathway; GCM, Global climate model.

YRB. Maize yield exhibits basin-wide declines under SSP245 and SSP585, with reductions strengthening from SSP126 to SSP585 and from northwest to southeast (Fig. 3a). For wheat, spring wheat generally declines under climate change, especially in the northern YRB (e.g., the Hetao Irrigation District), but winter wheat yield tends to increase under climate change. The time series indicates that maize yield increases slightly before 2040 s, then will declines reaching 0–15 % (SSP126), 1.0–22.6 % (SSP245), and 11.2–35.5 % (SSP585) compared with baseline by 2099 (Fig. 3b). Wheat yield increases through mid-century, but the rate slows after 2040 s, and under SSP585 yields begin to decline after the 2070 s. By 2099, wheat yield changes range around −2.8–6.8 % (SSP126), −6.5–9.6 % (SSP245), and −15.0–4.8 % (SSP585) compared to 1980–2010. Spatiotemporal patterns for soybean and rice are shown in Figure S1. Soybean yield generally increases in the western and northeastern YRB but decreases in the middle and lower reaches, with pronounced losses downstream under SSP585; rice occupies limited areas in the YRB but exhibits substantial declines under climate change.

3.2. Projected crop yield gap change

Because total yield change under climate change integrates multiple influences (precipitation, temperature, and CO_2 effect), it is difficult to isolate water limitation from yield changes alone. Therefore, we use the irrigated–rainfed yield gap to quantify drought-induced yield losses (Figures 4 and S2). The spatial patterns of yield-gap change differ from those of total yield change. For all four crops, yield gaps generally decrease from the upper to the lower reaches of the YRB, highlighting upstream drought-limitation hotspots (Figures 4 and S2). Across different scenarios, maize and soybean show the largest gaps under SSP585, followed by SSP245 and SSP126 (Figure 4b and S2b). Wheat exhibits a weaker or mixed scenario signal, whereas rice shows the largest increases under SSP585, followed by SSP126 and SSP245. Time-series results (1980–2099) indicate increasing yield gaps for maize and soybean with rates ordered SSP585 > SSP245 > SSP126; wheat decrease through mid-century and then increases after around 2040–2050.

3.3. Sensitivity analysis

3.3.1. Relative importance of different climate variables

To identify the dominant drivers of the yield gap under water limitation, we quantified the contributions of precipitation, ET, SPEI, and CO_2 to quantifying the contribution of each variable to yield gap. Precipitation represents water supply; ET serves as a proxy for atmospheric water demand; SPEI integrates supply and demand to indicate drought intensity; and CO_2 can modulate photosynthesis and water-use efficiency (WUE), especially in C_3 crops. For maize and soybean, SPEI is the main factor (Figure 5 and S4), although its importance declines from SSP126 to SSP585. Precipitation also exerts a strong influence, particularly under SSP126. The importance of CO_2 increases from SSP126 to SSP585, consistent with a potential CO_2-driven increase in crop water-use efficiency (WUE), with a larger increase for wheat and soybean than for maize. For spring wheat, precipitation dominates the yield gap and tends to strengthen in 2069–2099 under SSP126 and SSP245, but weakens under SSP585. For winter wheat, SPEI dominates in the baseline and declines in 2069–2099 under SSP126 and SSP245 (Figure S3). Across different crops, ET shows relatively higher importance in the baseline (1980–2010) and under SSP585 (2069–2099), but lower importance under SSP126 and SSP245. Although rice occupies limited areas in the YRB, its yield gap is mainly driven by precipitation and CO_2; the relative importance of CO_2 increases in the future, but the importance of precipitation declines, and ET increases the influence of the rice yield gap (Figure S5).

3.3.2. Trends in climatic sensitivity of yield gaps

To assess how climate drives drought-related yield losses, we estimated the climatic sensitivity of the yield gap with the DLM (Figure S6-S9). Sensitivities are generally small in the historical period, consistent with a milder climate state and variability that kept crops farther from stress. In contrast, the rate and magnitude of climate change are expected to intensify over the coming decades, especially in 2069–2099, leading to greater sensitivities (Li et al., 2019; Wang et al., 2022a; Yao et al., 2020). In the future period, precipitation is mostly negative with the yield gap (more rain with a smaller gap), and its magnitude tends to weaken under SSP585, particularly in the upstream of the YRB. ET

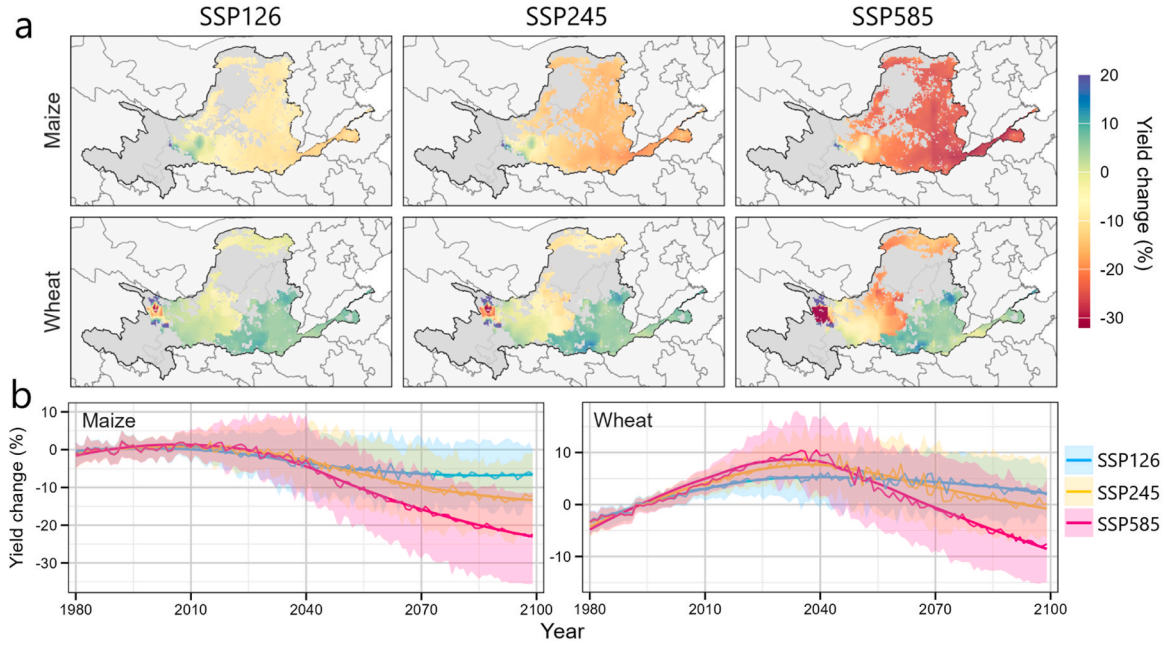

Fig. 3. Relative changes in crop yields from 1980 to 2099 in the Yellow River Basin under climate change. a, Spatial patterns of maize and wheat yield changes during 2069–2099 compared with the baseline period (1980–2010) under SSP126, SSP245, and SSP585 scenarios. b, Time series of maize and wheat yield changes from 1980 to 2099. Shaded areas represent the 20th-80th percentile range across 38 global climate models (GCMs) and nine crop models.

shows a positive association with the yield gap (higher atmospheric demand with larger gap), strongest under SSP245 and weaker under SSP126 and SSP585. SPEI is generally negatively associated with the yield gap, especially for maize, but it exhibits pronounced spatial heterogeneity across the basin (Figure S7). CO_2 sensitivities are also negative, indicating that higher CO_2 (via improved WUE) reduces the yield gap. Notably, CO_2 sensitivity is strongest under SSP245 during 2069–2099 (Figure S6-S9), likely because CO_2 increases are modest under SSP126, whereas under SSP585, CO_2 may exceed the range where CO_2 fertilization continues to increase strongly.

We also evaluated trends in sensitivity over 1980–2099 across scenarios Fig. 6). The yield-gap sensitivity to precipitation increases over most of the basin, with localized decreases mainly in the downstream YRB. Note that because the precipitation-yield gap relationship is negative, an increasing trend indicates a weakening in the absolute magnitude of sensitivity (shifts toward zero). The area fractions showing increasing trends are around 69.7 %, 66.7 %, and 77.8 % under SSP126, SSP245, and SSP585, respectively (Fig. 6b). In contrast, ET shows largely opposite patterns, with decreasing trends over approximately 65.8 %, 60.6 %, and 53.7 % of the YRB under SSP126, SSP245, and SSP585, respectively. For example, in the downstream YRB, the precipitation sensitivity shows a slight decreasing trend, whereas ET shows a pronounced increasing trend. The SPEI trend generally declines over most regions-about 67.4 %, 61.7 %, and 64.7 % show decreasing trends under SSP126, SSP245, and SSP585, with increases primarily concentrated in the western YRB. For CO_2, most areas display decreasing trends (approximately 70.5 %, 84.3 %, and 92.8 % under SSP126, SSP245, and SSP585), and the trend magnitude tends to increase from the western toward the eastern YRB.

For the other crops (wheat, soybean, and rice), spatial-temporal patterns similar to those of maize (Figs. S10-S12). For wheat, precipitation sensitivity shows increasing trends over 61.9 %, 55.5 %, and 64.3 % of the YRB under SSP126, SSP245, and SSP585, respectively, while ET sensitivity shows decreasing trends over 73.8 %, 69.9 %, and 66.6 %. SPEI sensitivity generally decreases across most regions (77.8 %, 73.1 %, and 65.8 % with decreasing trends under SSP126, SSP245, and SSP585), and CO_2 sensitivity also decreases in around 87–90 % of the basin across scenarios. A notable exception is soybean, for which ET sensitivity increases across most regions.

3.4. Uncertainty of yield gap predictions

To summarize uncertainty across the ensemble, we use the coefficient of variation (CV) to characterize spread in the irrigated-rainfed yield gap (Fig. 7). Spatially, maize shows higher CV in the southern YRB, whereas wheat uncertainty is greater toward the western basin. For time series, maize CV declines steadily from around 0.76–0.78 in the historical period to around 0.65–0.75 by the late century among the three scenarios. It is perhaps because, as systems become increasingly water-limited, responses across models become more similar. In contrast, wheat exhibits a U-shaped change into mid-century and then rises after around 2060, with the largest late-century increase under SSP585 (from around 0.52–0.54–0.56–0.66, among three scenarios). For soybean and rice, CV also tends to decrease toward the end of the century (Figure S13). Notably, CV provides an overall measure of ensemble spread but does not separate the relative contributions of crop models, climate models, or their interactions, and we did not apply uncertainty-constraining approaches in this study.

4. Discussion

4.1. Climate change impact on food security

Our study projects high-resolution crop yield changes in the YRB and finds substantial declines under climate change, especially under SSP585. Since the recent climate trajectory most closely tracks SSP585 (Schwalm et al., 2020), avoiding impacts will require aggressive adaptation to increase the resilience of the food system (Peng and Guan, 2021). For maize, soybean, and rice, the irrigated-rainfed yield gap increases under different scenarios (Fig. 4 and Figure S2), indicating heightened drought risk. In the future period, the drought and heat risks substantially increased (Li et al., 2019; Xu et al., 2024), making irrigation essential for food security and buffer effects by providing on-demand water and mitigating dry-heat stress via sustained transpiration and canopy cooling (Wang et al., 2021; Yao et al., 2025a). In contrast, wheat shows a weaker and mixed scenario signal, likely because winter and spring wheat grow in different seasons and therefore experience different seasonal precipitation changes. Winter wheat shows a slight reduction in the yield gap, likely because it grows during the cool season when ET is lower and projected precipitation increases can buffer water stress, even as mean temperature increases. Spring wheat shows slightly increasing yield gaps because warming intensifies hot, dry conditions in late spring and summer, increasing drought risk. Such spatial patterns are generally consistent with previous crop-yield projection studies (Hou et al., 2024; Wei et al., 2025), although the magnitudes differ, likely due to differences in the crop and climate models used.

4.2. Climatic sensitivity to yield gaps

We assessed the relative importance of climatic drivers and found clear spatial heterogeneity: different regions are dominated by different variables in explaining the irrigated-rainfed yield gap. In the upstream of YRB (e.g., the Hetao Irrigation District), ET is the dominant factor. It is perhaps because high Vapor Pressure Deficit (VPD) and relatively low precipitation limit recharge of root-zone soil moisture from rainfall. Moreover, widespread soil salinity further reduces plant-available water, making production heavily dependent on irrigation (Sun et al., 2016; Zhao et al., 2025). For different scenarios, ET is projected to increase with warming, especially under SSP585 (Kim et al., 2021). Thus, in irrigation-dependent areas, ET increases the dominance of the yield gap (Fig. 5 and Figure S3-S5). Consequently, food production in these regions will increasingly rely on irrigation. In the middle reaches of the YRB, precipitation dominates the yield gap. It is because the summer monsoon impacts the timing and amount of root-zone recharge, with relatively low VPD (Liu et al., 2021), that rainfall anomalies have a more effective impact on crop growth. In addition, the soil-hydrologic setting, particularly in the eastern YRB, exhibits higher θs (saturated water content) and moderate θr (residual water), indicating a higher field capacity and likely larger plant-available water than the salinized soil of Hetao (Tong et al., 2024). Thus, precipitation is converted more efficiently into root-zone recharge. Under the SSP126 and SSP245, precipitation remains the dominant control because the increase in potential evaporative demand is modest, and ET does not become the binding constraint (Collignan et al., 2023; Rouholahnejad Freund and Kirchner, 2017). Consequently, changes in the aridity index (PET/P) are small and largely precipitation-driven, and ET is not the binding constraint in these scenarios. In the lower YRB, where rainfall is more abundant and high infiltration (Li et al., 2020), and loam-silt-loam soils provide substantial plant-available storage (Zhao et al., 2017). Therefore, the irrigated-rainfed yield gaps are smaller than in other regions, and the SPEI can better explain their variability than precipitation or ET al.one. Because both water supply (e.g., precipitation) and atmospheric demand (e.g., ET) are relatively high, precipitation or ET by themselves cannot represent crop water status. Generally, identifying the dominant factors by region can help better understand how drought risk affects and more accurately interpret scenario-dependent impacts on yields.

The sensitivity of the irrigated-rainfed yield gap to climate drivers is dynamic under climate change. For precipitation, the negative sensitivity weakens (shifts toward zero) in much of the upper YRB, where the yield gap is largest, indicating a weakened marginal influence of rainfall on narrowing the gap. In the arid upstream, sodic (saline-sodic) soils

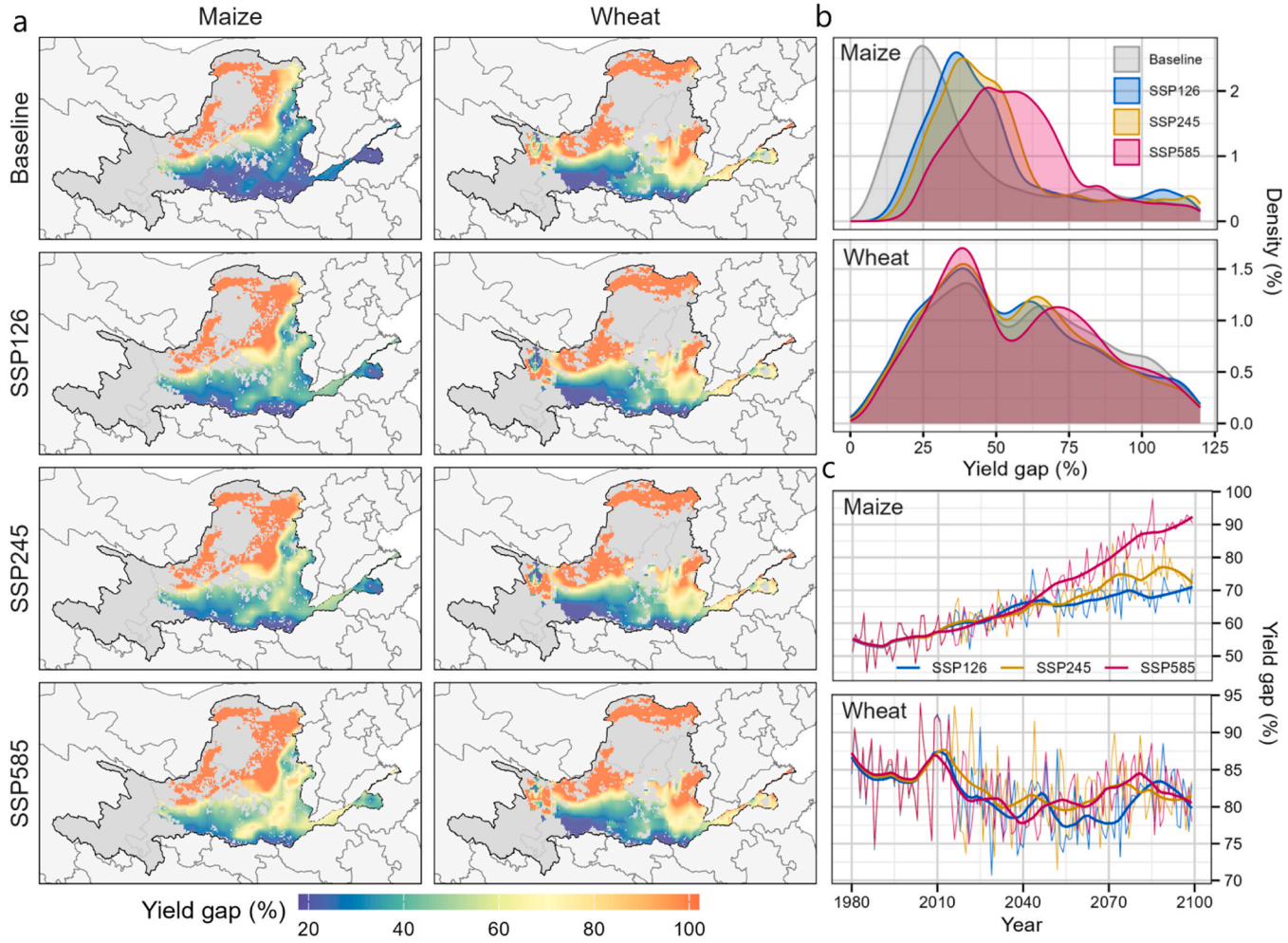

Fig. 4. Irrigated–rainfed yield gap for maize and wheat in the Yellow River Basin under historical and future climate scenarios based on the multi-model ensemble. a, Spatial patterns of yield gaps during the historical period (1980–2010) and future period (2069–2099) under SSP126, SSP245, and SSP585 scenarios. b, Density distributions of yield gaps for maize and wheat under different climate scenarios. c, Time series of yield gap changes from 1980 to 2099 for maize and wheat.

have lower infiltration capacity and plant-available water, while rising VPD accelerates post-rain soil-water drawdown, and such processes make rainfall less effective at recharging the root zone (Shrivastava and Kumar, 2015; Yuan et al., 2019). At the same time, higher atmospheric demand drives more soil evaporation from rainfall at the expense of root-zone recharge and transpiration, resulting in a concurrent decline in the marginal influence of both precipitation and ET on the yield gaps (Stoy et al., 2019; Zhang et al., 2017). Therefore, under these conditions, SPEI can integrate supply and demand, which more effectively captures the water conditions ((Fig. 6). By contrast, parts of the middle and lower YRB show a decreasing trend in precipitation sensitivity (more negative), indicating stronger precipitation-yield coupling and greater potential for rainfall to moderate the yield gap. In these regions, higher soil-water storage and increasing precipitation more effectively translate into root-zone moisture (Liu et al., 2024; Zhou et al., 2021). In addition, the increasing CO_2 can enhance plant growth while partially closing stomata, increasing water-use efficiency (WUE) that can improve the productivity return per millimeter of rain, especially in C_3 crops (Adams et al., 2021; Haverd et al., 2020; Toreti et al., 2020). Notably, the CO_2 fertilization signal is stronger in the arid upper basin (Fig. 6), where growth is most water-limited. Under such conditions, higher CO_2 raises WUE and allows each millimeter of rainfall to get a larger productivity gain than in less water-limited regions (Donohue et al., 2013; Zhang et al., 2022). However, our results indicate that the crop yield benefits from increased WUE have likely been offset by the intensification of drought in these regions. In addition, the benefit of CO_2-induced water savings depends on concurrent changes in evapotranspiration (ET) and atmospheric demand, which reflect coupled vegetation–climate interactions and are strongly regulated by multiple climatic drivers (Nkiaka et al., 2024).

4.3. Potential implications for sustainable development

Although irrigation is essential for food security (Rosa et al., 2020), it can increase greenhouse gas emissions directly from soils and indirectly from energy use, which highlights the need for sustainable irrigation (Yang et al., 2023). As climate change expands drought risk and reliance on irrigation, net atmospheric water influx to land may decline and potentially aggravate drought trends due to increased irrigation (Yao et al., 2025b). Therefore, targeted strategies are needed to mitigate these trade-offs. The spatial variability of ET under warming reflects shifts between water-limited and energy-limited regimes: in arid, water-limited regions, ET is constrained mainly by soil moisture and water supply, whereas in more energy-limited regions it responds more to available energy and moisture conditions (Nkiaka et al., 2024). Thus, these contrasts highlight the need for region-specific adaptation strategies. For example, in ET-dominated regions, shifting from continuous flooding and high-loss systems to alternate wetting and drying or mid-season drainage in rice, and from sprinkler to drip or micro-irrigation in upland crops, can reduce emissions while

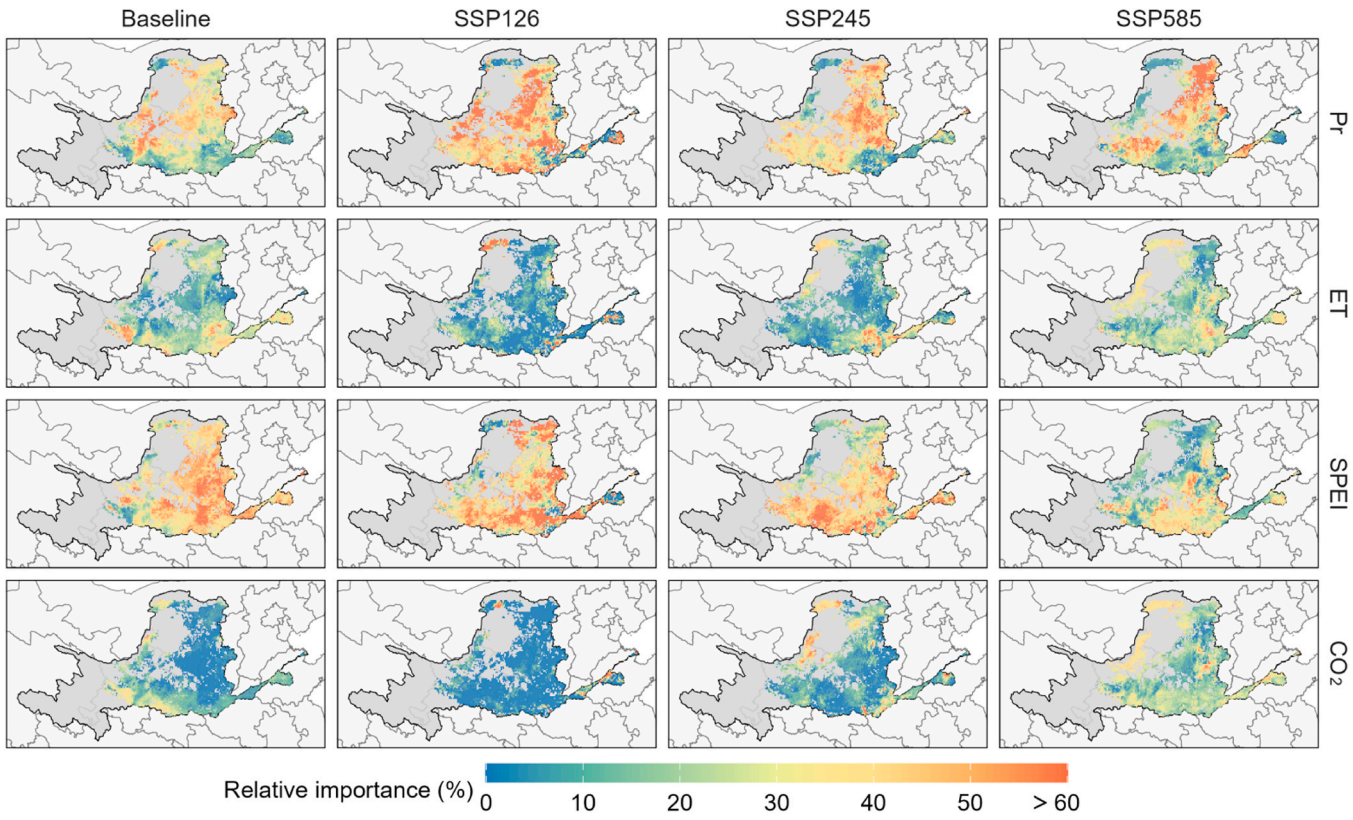

Fig. 5. Relative importance (%) of precipitation (Pr), evapotranspiration (ET), standardized precipitation-evapotranspiration index (SPEI), and atmospheric carbon dioxide concentration (CO_2) in explaining maize yield gap under the baseline (1980–2010) and future period (2069–2099) for SSP126, SSP245, and SSP585 scenarios.

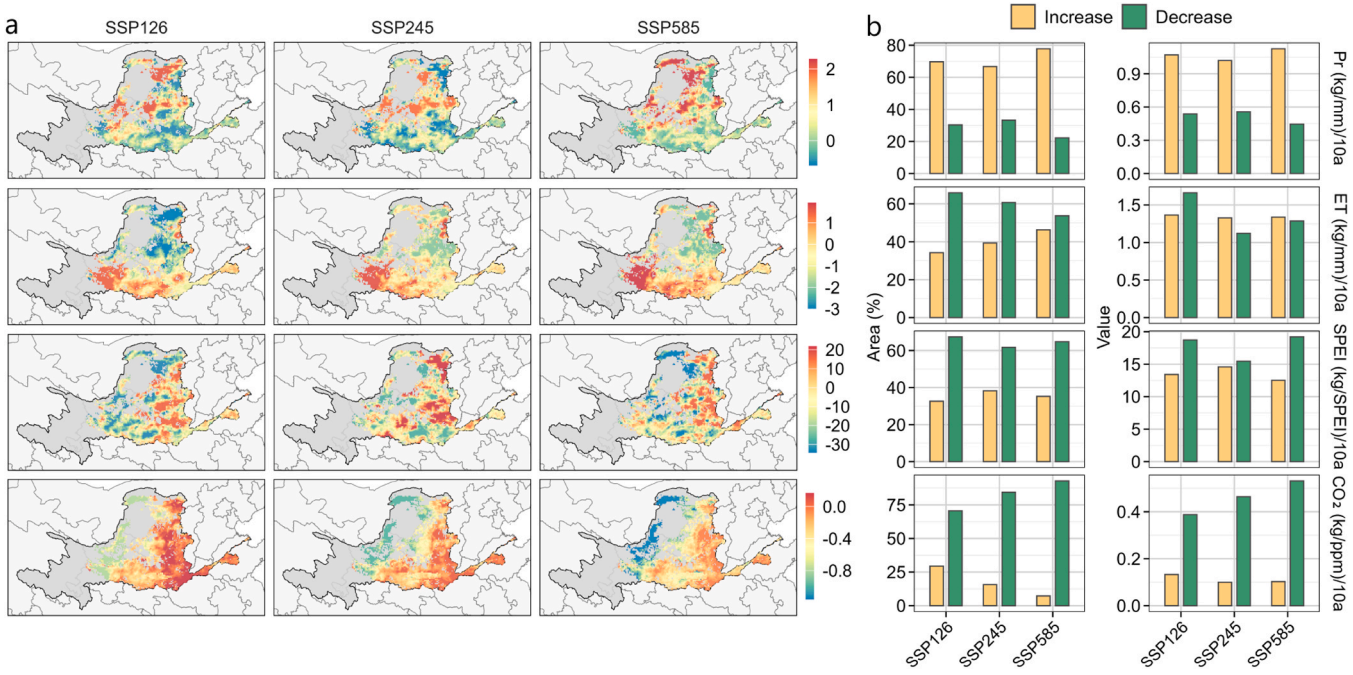

Fig. 6. Trends in the sensitivity of maize yield gaps to key climatic variables. a, Spatial patterns of the trends in maize yield gap sensitivity to precipitation (Pr), evapotranspiration (ET), standardized precipitation-evapotranspiration index (SPEI), and atmospheric carbon dioxide concentration (CO_2) under SSP126, SSP245, and SSP585 scenarios. b, Proportions of areas showing increasing or decreasing sensitivity. c, Mean sensitivity trends within regions of increase and decrease.

maintaining yields (Kuang et al., 2021). In precipitation-dominated regions, invest in effective rainfall on-farm storage, in-field retention, soil structure, and apply key-stage supplemental irrigation when precipitation sensitivity is strongest. In addition, crop switching guided by our

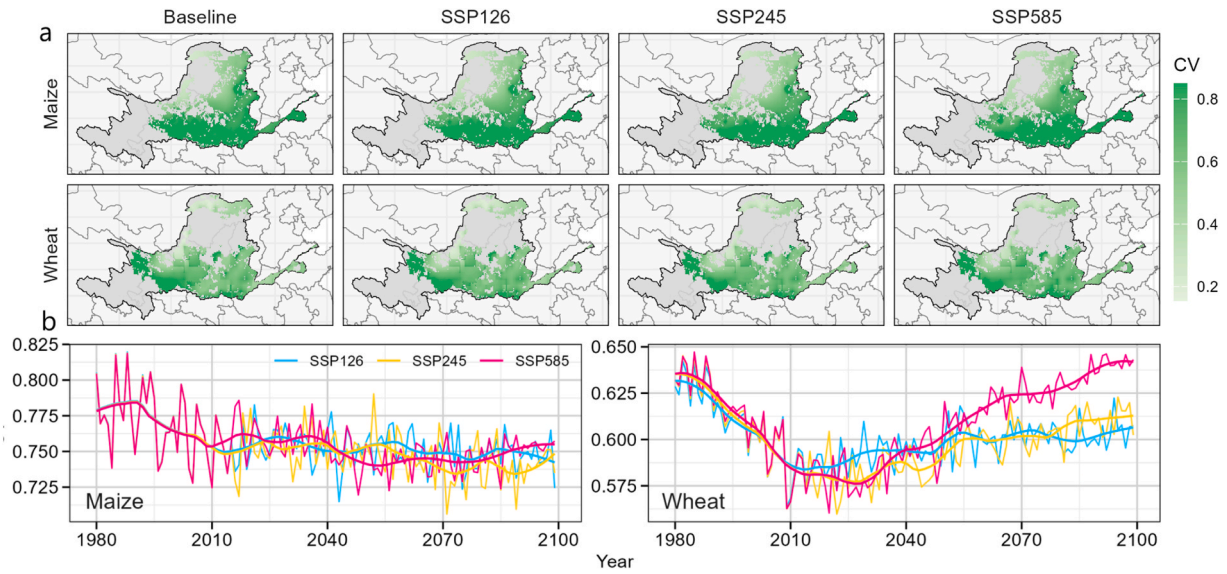

Fig. 7. Uncertainty in simulated crop yield gap projections is expressed as the coefficient of variation (CV) for maize and wheat in the Yellow River Basin. a, Spatial patterns of CV during the baseline period (1980–2010) and the future period (2069–2099) under SSP126, SSP245, and SSP585 scenarios. b, Time series of CV for maize and wheat from 1980 to 2099.

dominance maps can raise production while advancing sustainability co-benefits by reallocating planting toward climates where each crop's water climate sensitivities are more favorable (Chakraborti et al., 2023; Xie et al., 2023). Generally, by mapping where yield gaps expand and where sensitivities and their trends are strongest, together with regional dominance of key drivers, our results provide spatially explicit evidence to prioritize where and when irrigation and water-saving interventions are likely to be most effective, with potential co-benefits for reducing the greenhouse-gas intensity of production.

4.4. Limitations and way forward

This study has several limitations. First, extreme events can strongly affect yields, but we did not examine yield-gap sensitivity to specific extremes such as waterlogging (Kim et al., 2024) or flash drought (Otkin et al., 2018). Using growing-season means may mask short, high-impact episodes that alter the relationship between climate variables and the irrigated-rainfed gap. Second, crop yield projections still have large uncertainty (Li et al., 2023a; Müller et al., 2021) from climate models, process-based crop models, and their interaction(Wang et al., 2024a), which may affect the magnitude of projected yield-gap changes and sensitivity trends. In addition, the emulator-based climate-response functions are represented with saturating relationships, indicating the potential diminishing marginal effects at high driver levels. Consequently, under stronger forcing, further increases in climatic drivers may yield smaller incremental changes in the yield gap, affecting the magnitude of scenario-dependent sensitivities. Third, while sustainable irrigation under climate change can advance the Sustainable Development Goals (SDGs), we did not evaluate specific irrigation strategies or their net greenhouse gas outcomes in this work. Our future study could focus on co-design and test sustainable irrigation portfolios that maintain yields under climate change while reducing greenhouse gas emissions, linking our sensitivity trend maps to actionable scheduling, technology choices, and policy instruments (McDermid et al., 2023; Yang et al., 2023; Zhang et al., 2021). Future work could also better represent short-term extremes by integrating sub-seasonal modeling or weather-generator outputs to simulate high-impact events (e.g., heat, flash droughts, and waterlogging) within the growing season. In addition, since soil organic carbon can buffer yield losses under warming (Feng et al., 2022; He et al., 2025), an important direction is to assess whether soil profile properties and carbon management can further mitigate drought risk under future climates.

5. Conclusion

This study uses the irrigated–rainfed yield gap to quantify drought risk in the Yellow River Basin under climate change. We estimate yield-gap sensitivities to key climatic drivers (precipitation, evapotranspiration, SPEI, and CO_2) and show that these sensitivities shift over time across SSP126, SSP245, and SSP585. Combined with projected crop yield changes and evolving irrigated-rainfed yield gaps, our results identify where drought-related yield losses are likely to intensify and where climatic impacts on the yield gap are strengthening or weakening. These spatial hotspots provide clear targets for locally adapted, scenario-aware irrigation and water-management planning. Since drought risk is increasing due to climate change, especially in the YRB, which depends heavily on irrigation, decision-makers need strategies that both improve resilience and support sustainable management. Our results provide spatially explicit evidence to support the prioritization of adaptation planning and to inform where and when irrigation is likely to deliver the greatest benefit, rather than prescribing operational “rules” directly. In particular, the sensitivity trend maps can help identify regions and periods in which supplemental water is most strongly associated with narrowing yield gaps, providing a quantitative basis for scenario-aware water management planning. These insights can potentially contribute to increasing the efficiency of climate-smart practices that stabilize production while advancing long-term sustainability goals.

CRediT authorship contribution statement

Guijun Yang: Writing – review & editing, Supervision, Investigation, Data curation, Conceptualization. **Qiang Yu:** Writing – review & editing, Validation, Funding acquisition, Conceptualization. **Hao Feng:** Writing – review & editing, Resources, Conceptualization. **Zhongshan Xu:** Writing – original draft, Methodology, Investigation, Formal analysis, Data curation, Conceptualization. **Yajie Zhang:** Visualization, Validation, Resources, Formal analysis, Conceptualization. **Ning Yao:** Writing – review & editing, Validation, Formal analysis, Data curation, Conceptualization. **Yi Li:** Writing – review & editing, Resources, Investigation, Data curation. **Qinsi He:** Writing – review & editing, Writing – original draft, Validation, Supervision, Resources, Project administration, Formal analysis, Data curation, Conceptualization. **Linchao Li:**

Writing – review & editing, Writing – original draft, Visualization, Validation, Software, Resources, Methodology, Investigation, Formal analysis, Data curation, Conceptualization.

Declaration of Competing Interest

The authors declare that they have no known competing financial interests or personal relationships that could have appeared to influence the work reported in this paper.

Acknowledgements

The study was supported by the National Natural Science Foundation of China (No. 42501370 and 42501067), Open Research Fund of the National Key Laboratory of Soil and Water Conservation and Desertification Control (No. Z2010025001-KJ2520), and funded by the Inner Mongolia Autonomous Region Education Special Fund Project (2025).

Appendix A. Supporting information

Supplementary data associated with this article can be found in the online version at doi:10.1016/j.agwat.2026.110137.

Data Availability

No data was used for the research described in the article.

References

Adams, M.A., Buckley, T.N., Binkley, D., Neumann, M., Turnbull, T.L., 2021. CO(2), nitrogen deposition and a discontinuous climate response drive water use efficiency in global forests. Nat. Commun. 12 (1), 5194.
Allan, R.P., et al., 2020. Advances in understanding large-scale responses of the water cycle to climate change. Ann. N. Y Acad. Sci. 1472 (1), 49–75.
Bo, Y., et al., 2024. Improved alternate wetting and drying irrigation increases global water productivity. Nat. Food.
Breiman, L., 2001. Random forests. Mach. Learn. 45 (1), 5–32.
Cao, J., et al., 2025. Mapping global yields of four major crops at 5-minute resolution from 1982 to 2015 using multi-source data and machine learning. Sci. Data 12 (1), 357.
Chakraborti, R., et al., 2023. Crop switching for water sustainability in India's food bowl yields co-benefits for food security and farmers' profits. Nat. Water 1 (10), 864–878.
Chen, X., et al., 2020. Impacts of multi-timescale SPEI and SMDI variations on winter wheat yields. Agric. Syst. 185.
Collignan, J., Polcher, J., Bastin, S., Quintana-Segui, P., 2023. Budyko Framework Based Analysis of the Effect of Climate Change on Watershed Evaporation Efficiency and Its Impact on Discharge Over Europe. Water Resour. Res. 59 (10).
Donohue, R.J., Roderick, M.L., McVicar, T.R., Farquhar, G.D., 2013. Impact of CO2 fertilization on maximum foliage cover across the globe's warm, arid environments. Geophys. Res. Lett. 40 (12), 3031–3035.
Feng, P., et al., 2022. Soil properties resulting in superior maize yields upon climate warming. Agron. Sustain. Dev. 42 (5).
Feng, P., Wang, B., Liu, D.L., Waters, C., Yu, Q., 2019. Incorporating machine learning with biophysical model can improve the evaluation of climate extremes impacts on wheat yield in south-eastern Australia. Agric. For. Meteorol. 275, 100–113.
Franke, J.A., et al., 2020b. The GGCMI Phase-2 emulators: global gridded crop model responses to changes in CO_2, temperature, water, and nitrogen (version 1.0). Geosci. Model Dev. 13 (9), 3995–4018.
Franke, J.A., et al., 2020a. The GGCMI Phase 2 experiment: global gridded crop model simulations under uniform changes in CO_2, temperature, water, and nitrogen levels (protocol version 1.0). Geosci. Model Dev. 13 (5), 2315–2336.
Greve, P., Seneviratne, S.I., 2015. Assessment of future changes in water availability and aridity. Geophys Res Lett. 42 (13), 5493–5499.
Haverd, V., et al., 2020. Higher than expected CO(2) fertilization inferred from leaf to global observations. Glob. Chang Biol. 26 (4), 2390–2402.
He, Q., et al., 2025. Soil organic carbon improvement for mitigating crop yield losses under global warming. Eur. J. Agron. 170.
Hou, M., et al., 2024. Concurrent drought threaten wheat and maize production and widen crop yield gaps in the future. Agric. Syst. 220, 104056.
Jägermeyr, J., et al., 2021. Climate impacts on global agriculture emerge earlier in new generation of climate and crop models. Nat. Food.
Kamali, B., et al., 2022. Probabilistic modeling of crop-yield loss risk under drought: a spatial showcase for sub-Saharan Africa. Environ. Res. Lett. 17 (2).
Kim, D., Ha, K.J., Yeo, J.H., 2021. New drought projections over east asia using evapotranspiration deficits from the CMIP6 warming scenarios. Earth's. Future 9 (6).
Kim, Y.-U., et al., 2024. Mechanisms and modelling approaches for excessive rainfall stress on cereals: Waterlogging, submergence, lodging, pests and diseases. Agric. For. Meteorol. 344.
Krishnamurthy R, P.K., Fisher, J.B., Choularton, R.J., Kareiva, P.M., 2022. Anticipating drought-related food security changes. Nat. Sustain. 5 (11), 956–964.
Kuang, W., Gao, X., Tenuta, M., Zeng, F., 2021. A global meta-analysis of nitrous oxide emission from drip-irrigated cropping system. Glob. Chang Biol. 27 (14), 3244–3256.
Leng, G., Hall, J., 2019. Crop yield sensitivity of global major agricultural countries to droughts and the projected changes in the future. Sci. Total Environ. 654, 811–821.
Li, L., et al., 2019. Future projections of extreme temperature events in different sub-regions of China. Atmos. Res. 217, 150–164.
Li, L., et al., 2020. Trends, change points and spatial variability in extreme precipitation events from 1961 to 2017 in China. Hydrol. Res.
Li, L., et al., 2022. Developing machine learning models with multi-source environmental data to predict wheat yield in China. Comput. Electron. Agric. 194.
Li, L., et al., 2023a. The optimization of model ensemble composition and size can enhance the robustness of crop yield projections. Commun. Earth Environ. 4 (1).
Li, L., et al., 2023b. Integrating machine learning and environmental variables to constrain uncertainty in crop yield change projections under climate change. Eur. J. Agron. 149.
Li, X., Troy, T.J., 2018. Changes in rainfed and irrigated crop yield response to climate in the western US. Environ. Res. Lett. 13 (6).
Liu, J., Jin, J., Niu, G.Y., 2021. Effects of irrigation on seasonal and annual temperature and precipitation over china simulated by the WRF Model. J. Geophys. Res. Atmosp. 126 (10).
Liu, Y., Kumar, M., Katul, G.G., Porporato, A., 2019. Reduced resilience as an early warning signal of forest mortality. Nat. Clim. Change 9 (11), 880–885.
Liu, Y., Chen, X., Bai, Y., Zeng, J., 2024. Evaluation of 22 CMIP6 model-derived global soil moisture products of different shared socioeconomic pathways. J. Hydrol. 636, 131241.
McDermid, S., et al., 2023. Irrigation in the Earth system. Nat. Rev. Earth Environ. 4 (7), 435–453.
Meehl, G.A., et al., 2020. Context for interpreting equilibrium climate sensitivity and transient climate response from the CMIP6 Earth system models. Sci. Adv. 6 (26), eaba1981.
Mehta, P., et al., 2024. Half of twenty-first century global irrigation expansion has been in water-stressed regions. Nat. Water 2 (3), 254–261.
Monfreda, C., Ramankutty, N., Foley, J.A., 2008. Farming the planet: 2. Geographic distribution of crop areas, yields, physiological types, and net primary production in the year 2000. Glob. Biogeochem. Cycles 22 (1) (n/a-n/a).
Müller, C., et al., 2021. Exploring uncertainties in global crop yield projections in a large ensemble of crop models and CMIP5 and CMIP6 climate scenarios. Environ. Res. Lett. 16 (3).
Niu, B., et al., 2024. Improved identification and monitoring of meteorological, agricultural, and hydrological droughts using the modified nonstationary drought indices in the Yellow River Basin of China. J. Hydrol. 643.
Nkiaka, E., et al., 2024. Quantifying the effects of climate and environmental changes on evapotranspiration variability in the Sahel. J. Hydrol. 642.
Otkin, J.A., et al., 2018. Flash droughts: a review and assessment of the challenges imposed by rapid-onset droughts in the United States. Bull. Am. Meteorol. Soc. 99 (5), 911–919.
Peng, B., Guan, K., 2021. Harmonizing climate-smart and sustainable agriculture. Nat. Food 2 (11), 853–854.
Peng, S., Ding, Y., Liu, W., Li, Z., 2019. 1 km monthly temperature and precipitation dataset for China from 1901 to 2017. Earth Syst. Sci. Data 11 (4), 1931–1946.
Portmann, F.T., Siebert, S., Döll, P., 2010. MIRCA2000-Global monthly irrigated and rainfed crop areas around the year 2000: a new high-resolution data set for agricultural and hydrological modeling. Glob. Biogeochem. Cycles 24 (1) (n/a-n/a).
Prado, R., West, M., 2010. Time series: modeling, computation, and inference. Chapman and Hall/CRC.
Rosa, L., et al., 2020. Potential for sustainable irrigation expansion in a 3 ° C warmer climate. Proc. Natl. Acad. Sci. USA 117 (47), 29526–29534.
Rouholahnejad Freund, E., Kirchner, J.W., 2017. A Budyko framework for estimating how spatial heterogeneity and lateral moisture redistribution affect average evapotranspiration rates as seen from the atmosphere. Hydrol. Earth Syst. Sci. 21 (1), 217–233.
Santini, M., Noce, S., Antonelli, M., Caporaso, L., 2022. Complex drought patterns robustly explain global yield loss for major crops. Sci. Rep. 12 (1), 5792.
Schwalm, C.R., Glendon, S., Duffy, P.B., 2020. RCP8.5 tracks cumulative CO(2) emissions. Proc. Natl. Acad. Sci. USA 117 (33), 19656–19657.
Shrivastava, P., Kumar, R., 2015. Soil salinity: A serious environmental issue and plant growth promoting bacteria as one of the tools for its alleviation. Saudi J. Biol. Sci. 22 (2), 123–131.
Stoy, P.C., et al., 2019. Reviews and syntheses: Turning the challenges of partitioning ecosystem evaporation and transpiration into opportunities. Biogeosciences 16 (19), 3747–3775.
Sun, S., et al., 2016. Comprehensive evaluation of water use in agricultural production: a case study in Hetao Irrigation District, China. J. Clean. Prod. 112, 4569–4575.
Swann, A.L., Hoffman, F.M., Koven, C.D., Randerson, J.T., 2016. Plant responses to increasing CO_2 reduce estimates of climate impacts on drought severity. Proc. Natl. Acad. Sci. USA 113 (36), 10019–10024.
Thornthwaite, C.W., 1948. An approach toward a rational classification of climate. Geogr. Rev. 38 (1), 55–94.
Tong, Y., et al., 2024. Dataset of soil hydraulic parameters in the Yellow River Basin based on in situ deep sampling. Sci. Data 11 (1).

Toreti, A., et al., 2020. Narrowing uncertainties in the effects of elevated CO_2 on crops. Nat. Food 1 (12), 775–782.
Wang, B., et al., 2024a. Pathways to identify and reduce uncertainties in agricultural climate impact assessments. Nat. Food.
Wang, B., et al., 2024b. Probabilistic analysis of drought impact on wheat yield and climate change implications. Weather Clim. Extrem. 45, 100708.
Wang, L., et al., 2022a. Projection of precipitation extremes in China's mainland based on the statistical downscaled data from 27 GCMs in CMIP6. Atmos. Res. 280.
Wang, S., et al., 2025. Anthropogenic impacts on the Yellow River Basin. Nat. Rev. Earth Environ. 6 (10), 656–671.
Wang, X., et al., 2021. Global irrigation contribution to wheat and maize yield. Nat. Commun. 12 (1), 1235.
Wang, Y., Wang, S., Zhao, W., Liu, Y., 2022b. The increasing contribution of potential evapotranspiration to severe droughts in the Yellow River basin. J. Hydrol. 605.
Wei, Y., et al., 2025. Strategies for mitigating winter wheat yield reduction in the Yellow River basin: simulations and insights from CMIP6 data and the improved DSSAT-CERES-wheat model. Agric. Water Manag. 318.
Xie, W., et al., 2023. Crop switching can enhance environmental sustainability and farmer incomes in China. Nature.
Xu, F., et al., 2024. Understanding climate change impacts on drought in China over the 21st century: a multi-model assessment from CMIP6. npj Clim. Atmos. Sci. 7 (1).
Yang, Y., et al., 2023. Sustainable irrigation and climate feedbacks. Nat. Food 4 (8), 654–663.
Yao, N., et al., 2020. Projections of drought characteristics in China based on a standardized precipitation and evapotranspiration index and multiple GCMs. Sci. Total Environ. 704, 135245.
Yao, Y., et al., 2025b. Irrigation-induced land water depletion aggravated by climate change. Nat. Water.
Yao, Y., et al., 2025a. Compounding future escalation of emissions- and irrigation-induced increases in humid-heat stress. Nat. Commun. 16 (1), 9326.
YRCC, 2019. Yellow River Conservancy Commission. Yellow River water resource bulletin 2004-2018, Zhengzhou, China. ⟨www.yellowriver.gov.cn⟩.
Yuan, W., et al., 2019. Increased atmospheric vapor pressure deficit reduces global vegetation growth. Sci. Adv. 5 (8) eaax1396.
Zhang, J., et al., 2021. Sustainable irrigation based on co-regulation of soil water supply and atmospheric evaporative demand. Nat. Commun. 12 (1), 5549.
Zhang, Y., et al., 2017. Global variation of transpiration and soil evaporation and the role of their major climate drivers. J. Geophys. Res. Atmospheres 122 (13), 6868–6881.
Zhang, Y., et al., 2022. Increasing sensitivity of dryland vegetation greenness to precipitation due to rising atmospheric CO2. Nat. Commun. 13 (1), 4875.
Zhao, Y., et al., 2017. Soil-water storage to a depth of 5 m along a 500-km transect on the Chinese Loess Plateau. Catena 150, 71–78.
Zhao, Y., et al., 2025. Inversion of soil salinization at the branch canal scale in the Hetao Irrigation District based on improved spectral indices. Agric. Water Manag. 316.
Zhou, S., et al., 2021. Soil moisture–atmosphere feedbacks mitigate declining water availability in drylands. Nat. Clim. Change 11 (1), 38–44.
Zhuo, L., et al., 2022. Volume versus value of crop-related water footprints and virtual water flows: A case study for the Yellow River Basin. J. Hydrol. 608.